PAXX Is an Accessory c-NHEJ Factor that Associates with Ku70 and Has Overlapping Functions with XLF

Satish K. Tadi, Carine Tellier-Lebègue, Clément Nemoz, Pascal Drevet, Stéphane Audebert, Sunetra Roy, Katheryn Meek, Jean-Baptiste Charbonnier, Mauro Modesti

Article

Cell Reports

PAXX Is an Accessory c-NHEJ Factor that Associates with Ku70 and Has Overlapping Functions with XLF

Graphical Abstract

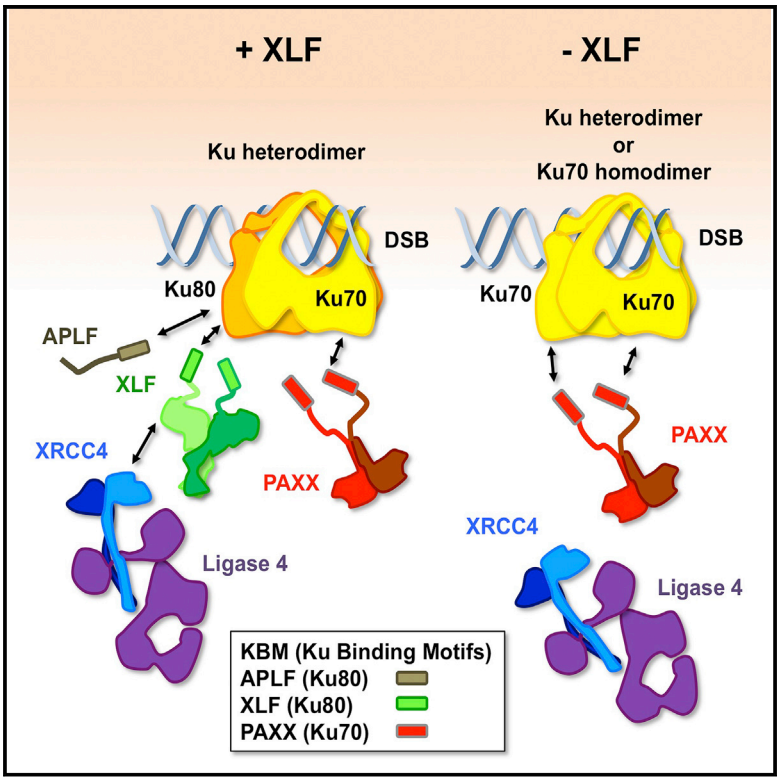

Highlights

- PAXX interaction with Ku threaded onto DNA requires a bare DNA extension
- PAXX interacts with the Ku70 subunit
- PAXX is dispensable for V(D)J recombination and has no core c-NHEJ phenotype
- PAXX's function in c-NHEJ is masked by XLF

Authors

Satish K. Tadi, Carine Tellier-Lebègue, Clément Nemoz, ..., Katheryn Meek, Jean-Baptiste Charbonnier, Mauro Modesti

Correspondence

mauro.modesti@inserm.fr

In Brief

Tadi et al. find that PAXX interacts with Ku threaded on DNA via the Ku70 subunit and requires a bare DNA extension for stability. They show that PAXX's function overlaps with c-NHEJ factor XLF, explaining why its ablation has only a mild effect on NHEJ.

Accession Numbers

PXD004659

Tadi et al., 2016, Cell Reports *17*, 541–555
October 4, 2016
http://dx.doi.org/10.1016/j.celrep.2016.09.026

Cell Reports
Article

PAXX Is an Accessory c-NHEJ Factor that Associates with Ku70 and Has Overlapping Functions with XLF

Satish K. Tadi,[1] Carine Tellier-Lebègue,[2] Clément Nemoz,[2] Pascal Drevet,[2] Stéphane Audebert,[1] Sunetra Roy,[3,4] Katheryn Meek,[3] Jean-Baptiste Charbonnier,[2] and Mauro Modesti[1,5,*]

[1]Cancer Research Center of Marseille, CNRS UMR7258, INSERM U1068, Institut Paoli-Calmettes, Aix-Marseille Université UM105, 13273 Marseille, France

[2]Institute for Integrative Biology of the Cell (I2BC), IBITECS, CEA, CNRS, University Paris-Sud, Université Paris-Saclay, 91198 Gif-sur-Yvette cedex, France

[3]Department of Microbiology & Molecular Genetics, and Department of Pathobiology & Diagnostic Investigation, College of Veterinary Medicine, Michigan State University, East Lansing, MI 48824, USA

[4]Present address: Department of Cancer Biology, The University of Texas, M.D. Anderson Cancer Center, Houston, TX 77054, USA

[5]Lead Contact

*Correspondence: mauro.modesti@inserm.fr

http://dx.doi.org/10.1016/j.celrep.2016.09.026

SUMMARY

In mammalian cells, classical non-homologous end joining (c-NHEJ) is critical for DNA double-strand break repair induced by ionizing radiation and during V(D)J recombination in developing B and T lymphocytes. Recently, PAXX was identified as a c-NHEJ core component. We report here that PAXX-deficient cells exhibit a cellular phenotype uncharacteristic of a deficiency in c-NHEJ core components. PAXX-deficient cells display normal sensitivity to radiomimetic drugs, are proficient in transient V(D)J recombination assays, and do not shift toward higher micro-homology usage in plasmid repair assays. Although PAXX-deficient cells lack c-NHEJ phenotypes, PAXX forms a stable ternary complex with Ku bound to DNA. Formation of this complex involves an interaction with Ku70 and requires a bare DNA extension for stability. Moreover, the relatively weak Ku-dependent stimulation of LIG4/XRCC4 activity by PAXX is unmasked by XLF ablation. Thus, PAXX plays an accessory role during c-NHEJ that is largely overlapped by XLF's function.

INTRODUCTION

DNA double-strand breaks (DSBs) are potentially cytotoxic lesions, as unrepaired or misrepaired DSBs can lead to chromosomal aberrations that have been shown to promote cancer and cell death (Deriano and Roth, 2013). Non-homologous end joining (NHEJ) performs the bulk of DSB repair in mammalian cells (Lieber, 2010). NHEJ can be further subdivided into classical NHEJ (c-NHEJ) and alternative NHEJ (a-NHEJ), involving distinct sets of proteins. The c-NHEJ pathway is versatile, ligating broken DNA ends with minimal end resection, while a-NHEJ is characterized by a dependence on micro-homologies exposed by resection of the broken ends before ligation (Chiruvella et al., 2013; Frit et al., 2014; Nussenzweig and Nussenzweig, 2007).

The core factors mediating c-NHEJ are the Ku70/80 heterodimer (Ku), DNA-dependent protein kinase catalytic subunit (DNA-PKcs), XRCC4, DNA Ligase 4 (LIG4), and XRCC4-like factor (XLF), also called Cernunnos or NHEJ1. These core factors are sufficient to recognize, align, and ligate a simple DSB. However, for complex or dirty breaks, additional accessory factors are required for DNA end processing before the final ligation (Akopiants et al., 2009; Ramsden and Asagoshi, 2012; Waters et al., 2014). Hallmarks of deficiencies in any of the core c-NHEJ factors include increased radiosensitivity, a shift in DSB repair toward a-NHEJ, and defects in somatic V(D)J recombination (Dudley et al., 2005; Fattah et al., 2014). The key components identified in a-NHEJ are DNA Ligase 3 (LIG3), poly(ADP-ribose) polymerase 1 (PARP1), and XRCC1, also known for their role in base excision repair (Audebert et al., 2006; Mansour et al., 2010). In cells deficient in LIG3, DNA Ligase 1 can substitute during a-NHEJ (Oh et al., 2014). It has been suggested that PARP1 competes with Ku for binding to broken DNA ends, thereby dictating pathway choice between repair by c-NHEJ versus a-NHEJ (Cheng et al., 2011; Wang et al., 2005), although in most cell types it would appear that c-NHEJ predominates.

Recently, three groups identified a factor involved in NHEJ known as Paralog of XRCC4 and XLF (PAXX; also denoted as C9orf142 or XLS) (Craxton et al., 2015; Ochi et al., 2015; Xing et al., 2015). PAXX was identified independently by a bioinformatics approach and by interactome analysis with human c-NHEJ factors. The crystal structures reveal that PAXX forms a homodimer through its N-terminal domain reminiscent of the XRCC4 and XLF homodimer structures. The major conclusions of these three studies are that (1) PAXX co-purifies with Ku and DNA-PKcs; (2) GFP-tagged PAXX is recruited to sites of laser micro-irradiation, co-localizing with Ku; (3) PAXX-deficient cells exhibit sensitivity to DSB-inducing agents; (4) by genetic epistasis analysis, PAXX functions in the same pathway as XLF for repairing dirty DSBs but

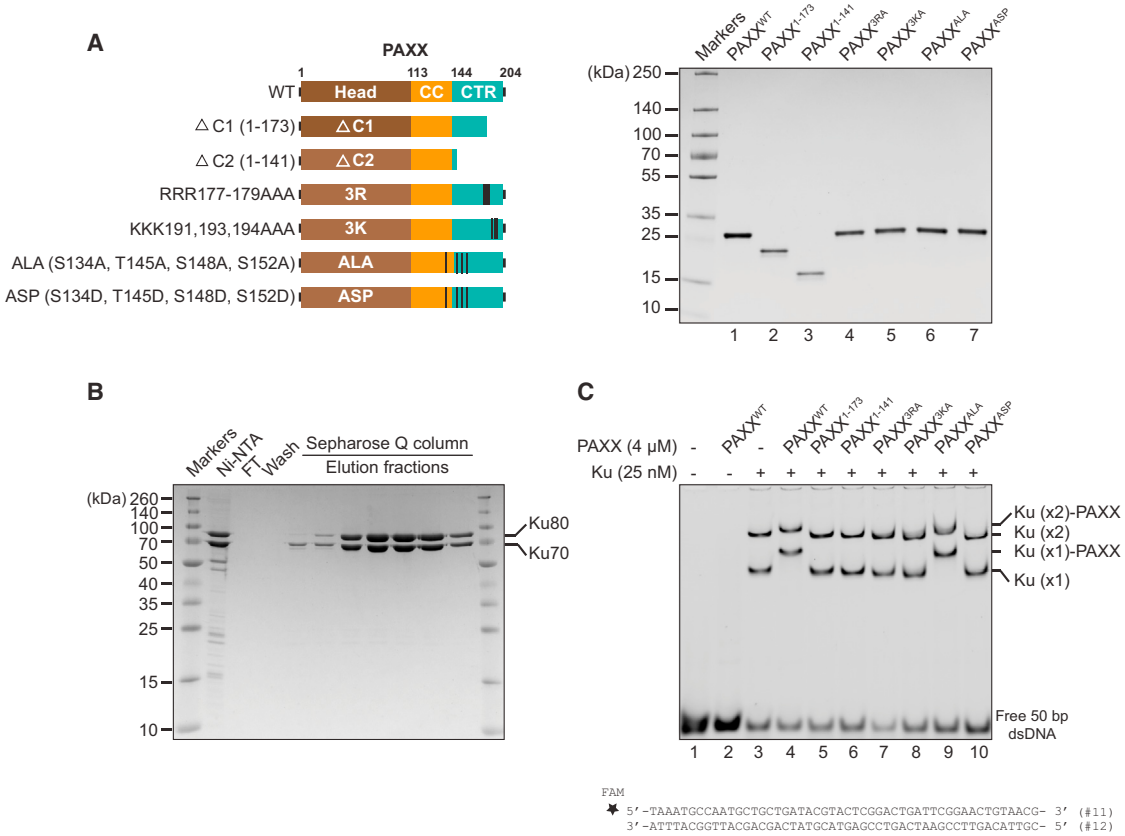

Figure 1. PAXX Forms a Ternary Complex with DNA-Bound Ku

(A) Schematic shows PAXX variant constructs (left panel) and Coomassie blue-stained reducing SDS-PAGE analysis of the purified PAXX proteins after over-expression in bacteria (right panel, ~3 μg/lane).

(B) Coomassie blue-stained reducing SDS-PAGE shows Ni-NTA and Sepharose Q column purification (peak fractions) of Ku produced in insect cells.

(C) EMSAs show super-shifting of Ku-DNA complexes by the PAXX variants using a 50-bp blunt-ended dsDNA with a 5′-6-carboxyfluorescein label (FAM).

independently of XLF in the case of simple breaks; and (5) recombinant PAXX associates with Ku-DNA complexes and stimulates the activity of the LIG4/XRCC4 complex in a Ku-dependent manner. From these observations, it was proposed that PAXX functions to promote assembly of the c-NHEJ machinery.

To help clarify the role of PAXX in DSB repair by NHEJ, we analyzed the in vitro activities of recombinant PAXX, including its interaction with DNA and Ku, and its effects in reconstituted core c-NHEJ reactions. Moreover, we studied PAXX's functional role in V(D)J recombination and a-NHEJ using PAXX-deficient human cells generated by CRISPR-Cas9-mediated genome editing. Collectively, our data indicate that PAXX is an accessory and not an obligate c-NHEJ factor and that it has overlapping functions with XLF.

RESULTS

PAXX Forms a Stable Ternary Complex with DNA-Bound Ku

To decipher how PAXX interacts with Ku and DNA, recombinant PAXX and Ku were produced in bacteria and insect cells, respectively (Figures 1A and 1B). Wild-type and a collection of PAXX variants were tested for DNA binding by electrophoretic mobility shift assays (EMSAs) using a 50-bp blunt-ended double-stranded DNA (dsDNA) (Figure 1C). Consistent with previous reports (Ochi et al., 2015; Xing et al., 2015), PAXX alone did not form stable complexes with DNA but super-shifted Ku-DNA complexes (Figure 1C, lanes 2–4). Deletions of the C-terminal tail of PAXX (ΔC1 or ΔC2) as well as point mutations of basic amino acids in these PAXX C-terminal tails (3RA, RRR177–179AAA; 3KA, KKK191–193–194AAA) completely abolished the ability of PAXX to super-shift Ku-DNA complexes (Figure 1C, lanes 5–8). In addition, the ASP phospho-mimetic variant (S134D, T145D, S148D, and S152D; identification of these phosphorylation sites is presented under accession number ProteomeXchange: PXD004659, reporting a PAXX interactome analysis; Figure S1; Table S1) also lost the ability to super-shift Ku-DNA complexes, but not the ALA variant (S134A, T145A, S148A, and S152A) (Figure 1C, lanes 9 and 10). Collectively, these results indicate that PAXX forms a complex with DNA-bound Ku. The stability of this ternary complex depends on the C-terminal tails of PAXX and might be regulated by phosphorylation.

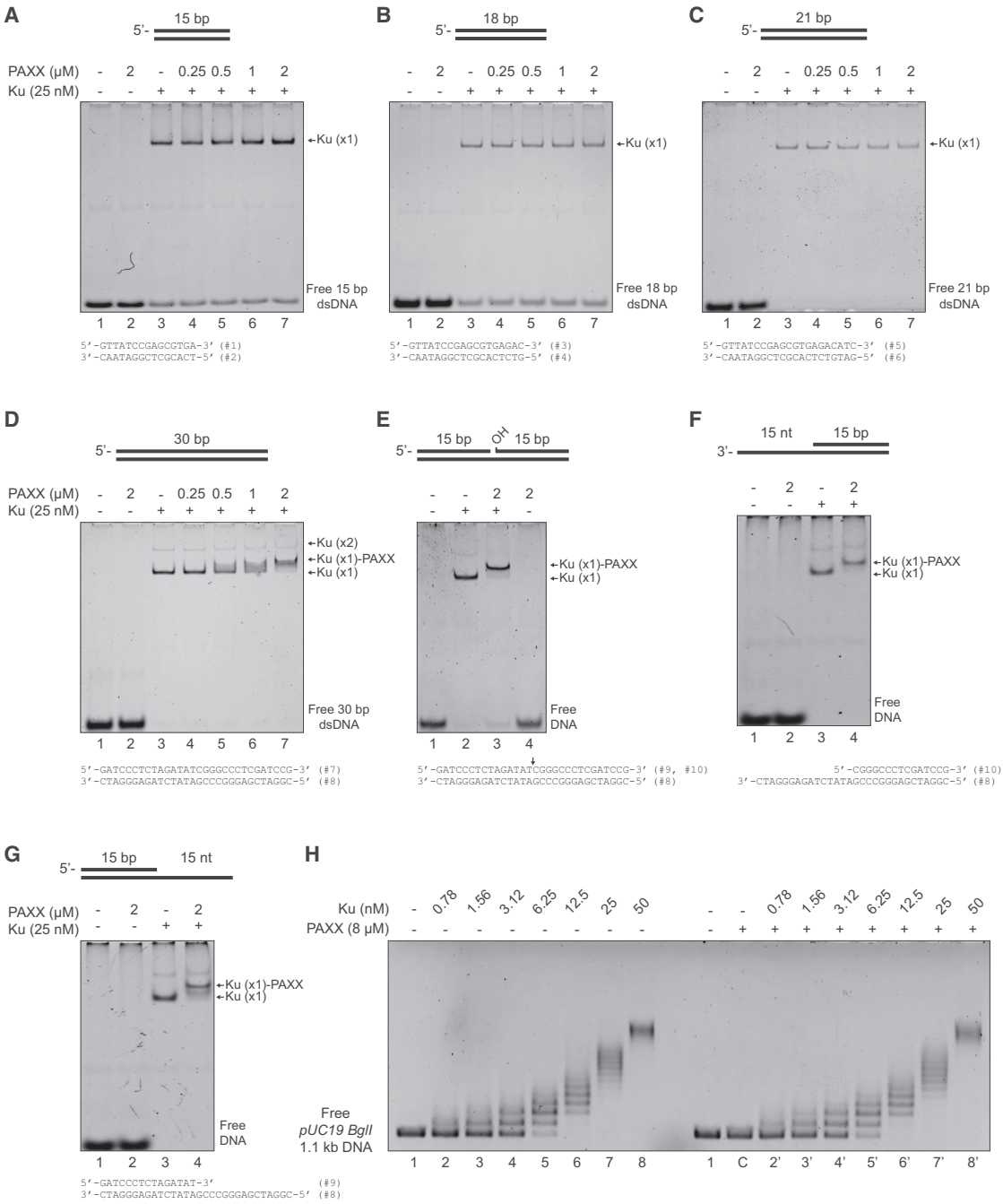

Figure 2. Stable PAXX-Ku-DNA Ternary Complex Requires a Stretch of Bare DNA

(A–H) EMSAs with PAXX and Ku using short dsDNA substrates of increasing length of 15, 18, 21, and 30 bp, respectively (A–D), a 30-bp substrate with a central nick (E), a 15-bp substrate with a 3′ (F) or 5′ (G) ssDNA overhang, and a large 1.1-kb DNA fragment (H) obtained by digestion of pUC19 with *BglI*.

PAXX Association with Ku-Bound DNA Requires a Ku-Free DNA Extension

To better understand the organization of PAXX-Ku-DNA ternary complexes, Ku-DNA super-shifting by PAXX was tested using short blunt-ended DNA substrates of 15, 18, and 21 bp (the DNA footprint of a Ku heterodimer is 14 bp; Yoo et al., 1999). With such short substrates, only one Ku heterodimer stably binds DNA; to our surprise, PAXX did not stably associate with these Ku-DNA complexes (Figures 2A–2C). However, when the size of the DNA substrate was increased to 30 bp, PAXX stably associated in a ternary complex with Ku-DNA (Figure 2D), indicating that 10–15 bp of bare

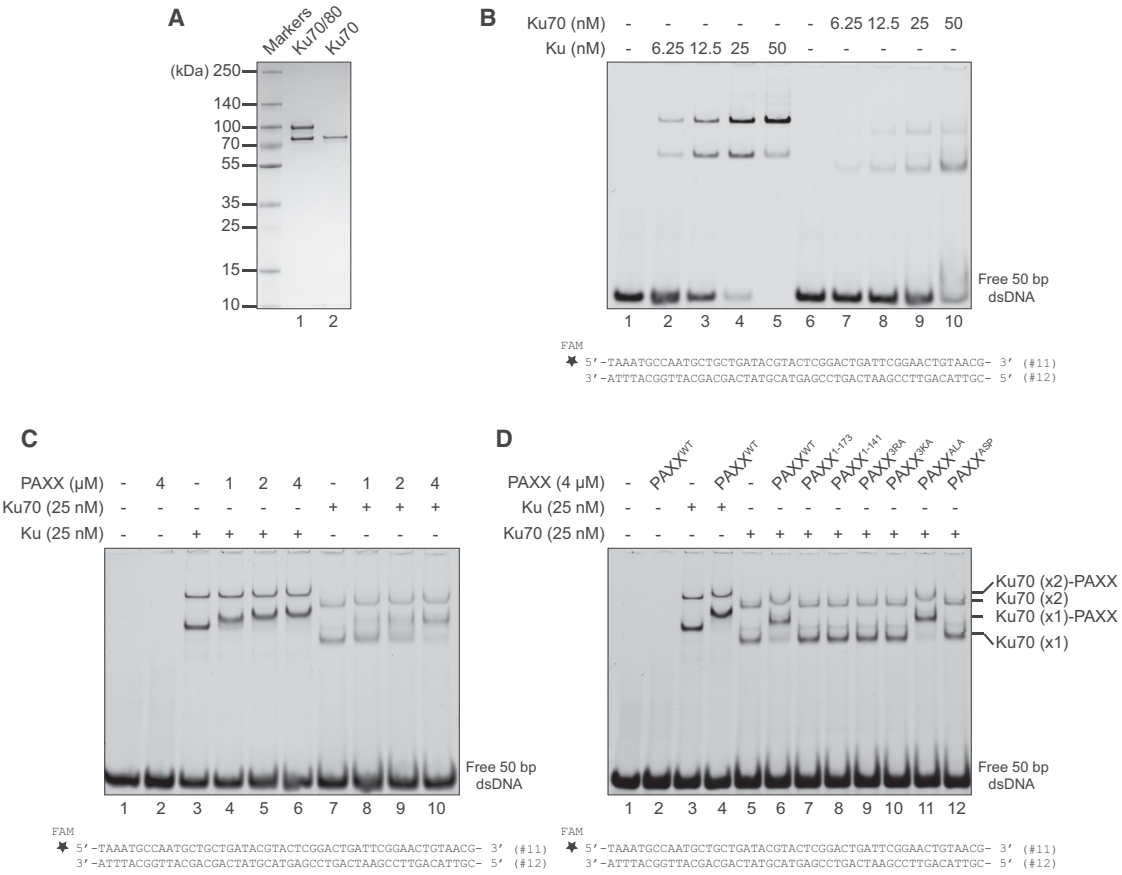

Figure 3. PAXX Super-Shifts DNA-Bound Ku70

(A) Coomassie blue-stained reducing SDS-PAGE analysis of purified Ku and Ku70 (~1 μg/lane) is shown.

(B) EMSAs show binding of Ku or Ku70 to a 5′-6-carboxyfluorescein-labeled (FAM) 50-bp blunt-ended dsDNA.

(C) EMSAs show super-shifting of DNA-bound Ku or Ku70 by PAXX.

(D) EMSAs show super-shifting of Ku70-DNA complexes by the PAXX variants, as in Figure 1C.

DNA protruding from Ku helps stabilize the ternary complex. The presence of a nick in the center of the 30-bp DNA substrate did not affect PAXX-Ku-DNA complex formation (Figure 2E). Remarkably, PAXX super-shifted Ku bound to a 15-bp dsDNA with 15-nt 3′ or 5′ single-stranded DNA (ssDNA) overhangs, but it did not exhibit affinity for these substrates on its own (Figures 2F and 2G). Similar results were obtained with a substrate containing a poly(dT) ssDNA tail, eliminating the possibility of secondary structure formation (Figures S2A and S2B).

Similar EMSAs using a large 1.1-kb dsDNA were performed to test whether PAXX could affect the loading of multiple Ku units onto DNA (Figure 2H). After pre-incubation of the DNA substrate with a large excess of PAXX, the loading of multiple Ku units on the DNA substrate was not affected, suggesting that PAXX does not prevent Ku's translocation from DNA ends to more inward positions on the DNA. These results indicate that the stable interaction of PAXX with Ku is strictly DNA dependent and also specifically requires a short stretch of bare DNA, not covered by the Ku heterodimer, which can be either single or double stranded.

PAXX Interacts with DNA-Bound Ku70 on a Site Remote from the APLF-Binding Site

As a first step toward understanding the protein-protein and protein-DNA contacts involved in PAXX-Ku-DNA ternary complex dynamics, we tested whether PAXX could interact with the Ku70 subunit of Ku, as Ku70 alone can bind to DNA in the absence of Ku80 (Allaway et al., 1990; Wang et al., 1994, 1998a, 1998b). The DNA-binding activity of purified recombinant Ku70 subunit and Ku from insect cells was first compared by EMSA as described above (Figures 3A and 3B). Ku70 alone stably bound to DNA, forming two shifted complexes with the 50-bp dsDNA substrate, though with an apparent lower affinity than the Ku heterodimer (Figure 3B). Next, the binding of PAXX to Ku70-DNA complexes was assessed (Figure 3C). PAXX forms a stable ternary complex with Ku70-DNA. To further verify that PAXX interacts with Ku70-DNA complexes, EMSAs were performed with the Ku70 subunit and the PAXX variants described previously. The binding of the PAXX variants to Ku70-DNA complexes matched that observed with Ku-DNA (compare Figures 1C and 3D). These results suggest that a PAXX-Ku70 protein-protein contact is involved in the formation of a stable PAXX-Ku-DNA ternary complex.

Table 1. Characterization of PAXX Interactions with Ku-DNA Complexes by Micro-calorimetry

N°	ITC Cell	ITC Syringe	K_a (10^5 M)	K_d (μM)	ΔH° (kcal/mol)	−TΔS° (kcal/mol)	ΔG° (kcal/mol)	Observation	Thermogram
1	Buffer	PAXX	no signal					no dissociation of PAXX dimer	Figure S3A
2	Ku	PAXX	NI	NI	NI	NI	NI	PAXX versus Ku heterodimer without DNA	Figure S3B
3	DNA (42 bp)	PAXX	NI	NI	NI	NI	NI	PAXX versus DNA	Figure S3C
4	Ku-DNA (42 bp) 1:1.1	PAXX	2.5 ± 0.2	4.1 ± 0.4	−9.4 ± 0.9	2.0 ± 0.9	−7.4 ± 0.2	one Ku heterodimer on the 42-bp DNA	Figure S3D
5	Ku-DNA (42 bp) 2:1.1	PAXX	1.0 ± 0.2	10 ± 3	−35 ± 6	29 ± 6	−6.8 ± 0.2	two Ku heterodimers on the 42-bp DNA	Figure S3E
6	Ku-hDNA 1:1.1	PAXX	<0.5	>20	weak			hDNA used for crystal structure	Figure S3F
7	Ku_{cc}-DNA (42 bp) 1:1.1	PAXX	3.1 ± 0.3	3.3 ± 0.4	−7.9 ± 0.5	0.4 ± 0.5	−7.5 ± 0.1	Ku_{cc} deleted Cter Ku70 and Cter Ku80	Figure S3G
8	Ku_{cc}-DNA (42 bp) 1:1.1	peptide PAXX	12.9 ± 0.4	0.8 ± 0.2	−22.6 ± 0.2	14.1 ± 0.2	−8.3 ± 0.2	peptide PAXX residues 178–204 RRRCPGESLINPGFKS KKPAGGVDFDET	Figure S3H
9	Ku_{cc}-hDNA 1:1.1	PAXX	<0.1	>100	weak			hDNA used for crystal structure	Figure S3I
10	Ku_{cc}-DNA F (15 bp–15 ss) 1:1.1	PAXX	1.9 ± 0.2	5.6 ± 0.5	−10 ± 2	3 ± 2	−7.0 ± 0.1	3′ ssDNA extension see Figure 2F	Figure S3J
11	Ku_{cc}-DNA G (15 bp–15 ss) 1:1.1	PAXX	1.7 ± 0.3	6.2 ± 0.9	−11 ± 7	3 ± 7	−7.1 ± 0.2	5′ ssDNA extension see Figure 2G	Figure S3K
12	$(Ku70)_2$-DNA (42 bp) 1:1.1	PAXX	29 ± 3	0.40 ± 0.04	−7.1 ± 0.2	−1.6 ± 0.2	−8.8 ± 0.2	Ku70 homodimer (insect cells)	Figure S3L
13	$(Ku70)_2$-DNA (42 bp) 1:1.1	PAXX	17 ± 5	0.6 ± 0.2	−1.9 ± 0.2	−6.6 ± 0.2	−8.5 ± 0.2	Ku70 homodimer (bacteria)	Figure S3M
14	Ku-DNA (42 bp)-pAPLF 1:1.1:1.1	PAXX	2.4 ± 0.4	4.3 ± 0.7	−7.9 ± 0.7	0.6 ± 0.8	−7.3 ± 0.2	no competition with APLF peptide 174–191, KQQPILAERKRILPTWML	Figure S3N

Accompanying EMSAs and representative thermograms are reported in Figure S2 and S3. All ITC experiments in this study were realized at 25°C. NI means no interaction, small and constant signal due to the dilution of the molecules injected in the cell. Weak indicates weak interaction that cannot be determined in the conditions used, a lower range of the K_d is proposed. The error is the deviation to the mean value of at least two measurements.

We further analyzed the interaction of PAXX with Ku, with DNA, and with Ku-DNA complexes by isothermal titration calorimetry (ITC). We first measured the heat exchange following PAXX injection into a micro-calorimeter cell containing the buffer, Ku, or a 42-bp blunt-ended dsDNA. We observed no heat exchange during these experiments (Table 1, lines 1–3; Figures S3A–S3C), suggesting that PAXX dimers do not dissociate and that PAXX has no detectable intrinsic affinity for DNA or for free Ku heterodimers in solution. We then measured the heat exchange during injection of PAXX into a cell containing Ku heterodimer and a 42-bp dsDNA in either a 1:1 or 2:1 stoichiometry. The EMSA experiments suggest that the complexes formed in these conditions consist primarily of one or two Ku heterodimers on the 42-bp dsDNA (Figure S2C). With the 1:1 stoichiometry, an enthalpy-driven interaction with a K_d of 4.1 ± 0.4 μM was observed between PAXX and the pre-formed 1:1 Ku-DNA complex (Table 1, line 4; Figure S3D). In contrast, with the 2:1 Ku:DNA stoichiometry, the enthalpy-driven reaction was ~2.5-fold weaker (K_d = 10 ± 3 μM) (Table 1, line 5; Figure S3E). These ITC data are consistent with EMSA data demonstrating stronger affinity of PAXX for the 1:1 Ku-DNA complex than for the 2:1 stoichiometry (Figure S2C).

These results suggest that PAXX may cooperatively bind to Ku and DNA protruding out of the Ku ring. At opposite, the data suggest no increased affinity due to the presence of two motifs present on the PAXX dimer with two Ku heterodimers positioned on the same 42-bp dsDNA. We performed similar experiments with the DNA substrate used to obtain a crystal structure of truncated Ku bound to DNA (Walker et al., 2001). This DNA has a hairpin on one DNA strand to orientate Ku binding. It is made of a 14-bp DNA duplex with a three-way junction comprising a 4-bp stem loop plus a short 5-nt G-rich stem region (referred to as hairpin DNA [hDNA]) (Figure S2D). PAXX has an at least 5-fold weaker affinity for this DNA covered by one Ku heterodimer than for the 42 bp substrate covered by one Ku heterodimer (Table 1, line 6; Figure S3F), confirming the cooperative binding of PAXX with DNA protruding out of the Ku heterodimer. The affinity observed with hDNA is >2-fold weaker compared to

the K_d measured for the 42 bp substrate covered by two Ku molecules. This last result suggests some steric hindrance between the hairpin and PAXX.

We then evaluated the role of the C-terminal regions of Ku70 and Ku80 in this interaction. We used a construct, Ku_{cc}, in which the C-terminal regions of both Ku70 and Ku80 were truncated (Ku_{cc} is a heterodimer containing residues 1–544 of Ku70 and residues 1–551 of Ku80, Figure S2E). PAXX also interacted with one Ku_{cc} bound to a 42-bp DNA with a K_d of 3.3 ± 0.4 μM, a similar affinity as that observed with full-length Ku in the same experimental conditions (Table 1, line 7; Figures S2F, S2G, S3G, and S3H). These data demonstrate that the C-terminal regions of Ku70 and Ku80 do not contribute significantly to Ku's interaction with PAXX. By titrating a peptide corresponding to PAXX C-terminal residues 178–204 into a cell containing one Ku_{cc} heterodimer per 42-bp DNA, we measured a 4-fold increase in affinity, K_d of 0.8 ± 0.2 μM, compared to the full-length PAXX homodimer (Table 1, line 8). This suggests that the PAXX C-terminal region drives its interaction with Ku, consistent with previous studies using PAXX C-terminal deletion mutants (Ochi et al., 2015; Xing et al., 2015; Figure 1C, lanes 5–8).

Using this minimal system, we further analyzed the interaction of PAXX with Ku_{cc} bound to various DNA substrates. As for the experiments with full-length Ku, the affinity of the interaction of PAXX with Ku_{cc} bound to the hDNA substrate was decreased (Table 1, line 9; Figure S3I). As detected in the EMSAs, the affinity of the interaction of PAXX with Ku_{cc} bound to a 15-bp dsDNA substrate with a 5′ or 3′ ssDNA was similar to that of PAXX for one Ku heterodimer bound to 42-bp DNA (Table 1, compare lines 4, 10, and 11; Figures 2F and 2G; Figures S2A, S2B, S3J, and S3K). The affinity of PAXX for one Ku70 homodimer bound to a 42-bp DNA was assessed. Affinities for DNA-bound Ku70, with K_d measurements of 0.40 ± 0.04 μM (Ku70 purified from insect cells) and 0.6 ± 0.2 μM (Ku70 purified from bacteria), were observed; these affinities are ~10- and 7-fold higher than that observed with the Ku heterodimer (Table 1, compare lines 4, 12, and 13; Figures S3L and S3M). These results confirm the EMSA experiments suggesting that PAXX's interaction site is on the Ku70 face and that the Ku70 homodimer can recapitulate the interaction observed with the Ku heterodimer. This provides a good explanation for the observation that a peptide derived from APLF, known to bind the Ku80 subunit (Grundy et al., 2016), does not affect Ku's interaction with PAXX (Table 1, line 14; Figure S3N). The interaction of this APLF peptide with Ku bound to DNA was measured by calorimetry, giving a K_d of 26 nM (C.N., unpublished data). We conclude that PAXX binds the Ku heterodimer on a site that is distinct from the site on Ku that can be occupied by APLF.

PAXX Stimulation of LIG4/XRCC4 Is Ku or Ku70 Dependent

XLF and Ku stimulate the ligation activity of the c-NHEJ LIG4/XRCC4 complex (Gu et al., 2007; Riballo et al., 2009; Tsai et al., 2007). To clarify the role of PAXX in the core c-NHEJ reaction, recombinant LIG4/XRCC4 complex and XLF expressed in bacteria were purified (Figure S4A). Using a blunt-ended DNA-ligation assay, we first confirmed Ku-dependent stimulation of the LIG4/XRCC4 complex activity (Figure 4A). The intrinsic blunt-ended DNA ligation efficiency of LIG4/XRCC4 is weak, but the presence of Ku induced a slight increase in activity (Figure 4A, lanes 2 and 3). PAXX alone has no stimulatory effect but, in the presence of Ku, the stimulation is substantial (Figure 4A, lanes 4–11). The Ku-dependent stimulatory effect of PAXX reached a plateau at ~2- to 3-fold molar excess of PAXX dimers over Ku, inducing a >5-fold stimulation. Analysis of the PAXX variants affected in PAXX-Ku-DNA ternary complex formation further confirmed that PAXX stimulates LIG4/XRCC4 in a Ku-dependent manner (Figure S4B), as reported previously (Ochi et al., 2015; Xing et al., 2015). Surprisingly, the PAXX ASP phospho-mimetic variant that is deficient in super-shifting DNA-bound Ku was able to stimulate ligation of blunt-ended DNA by LIG4/XRCC4 to levels comparable to the wild-type protein. The functional relevance of PAXX phosphorylation on residues S134, T145, S148, and S152, identified by PAXX interactome analysis after overexpression in HEK293 cells, remains therefore undefined.

Next, XLF was included in the ligation assays (cohesive and blunt) to reconstitute the core c-NHEJ reaction. In cohesive end ligation, XLF potently stimulated the LIG4/XRCC4 activity independently of Ku (Figure 4B, lane 6). In contrast, Ku only had a weak stimulatory effect and PAXX had no effect (Figure 4B, lanes 7 and 8). When Ku and PAXX were added simultaneously, either in the presence or absence of XLF, the stimulation was marginal (Figure 4B, lanes 11 and 12). It thus appears that the role of PAXX in cohesive end ligation by LIG4/XRCC4 is negligible even in the presence of Ku. However, in blunt-end ligation, Ku-dependent stimulation by PAXX could be detected reproducibly, but it was weak and mostly hidden by the strong Ku-dependent stimulation by XLF (Figure 4C, lanes 9–12). Since Ku70 could have functions independent of Ku80 (Ouyang et al., 1997), ligation assays were performed replacing Ku with Ku70. Interestingly, the same trend was observed (Figures S4C and S4D), i.e., strong Ku70-dependent XLF stimulation of LIG4/XRCC4 and weaker stimulation by PAXX. Overall, these data indicate that the most potent ligation stimulator of blunt-ended DNA fragments by LIG4/XRCC4 is XLF; this stimulation can be observed with either the Ku heterodimer or with Ku70 homodimers.

PAXX Is Dispensable for c-NHEJ in Living Cells

Deficiencies in core c-NHEJ factors confer ionizing radiation sensitivity and severe combined immunodeficiency due to a failure to repair DSBs induced by the RAG endonuclease during V(D)J recombination (de Villartay, 2015; Woodbine et al., 2014). To assess a potential role for PAXX in V(D)J recombination, the PAXX gene was disrupted in HEK293 cells using CRISPR-Cas9 gene editing; as controls, genes encoding other core c-NHEJ factors also were disrupted (XRCC4, XLF, and LIG4) (Figure 5A; Table S2). As can be seen in Figure 5B, HEK293 cells lacking XRCC4, XLF, or LIG4 were hypersensitive to Zeocin, a bleomycin analog that induces DSBs; in contrast, PAXX-deficient clones displayed no hypersensitivity to Zeocin.

To assess whether PAXX facilitates either coding or signal end joining during V(D)J recombination, a transient, episomal red/blue fluorescent reporter system was utilized (Figure 5C; Neal et al., 2016). As expected XRCC4-, XLF-, and LIG4-deficient cells had profound deficits in joining both coding and signal

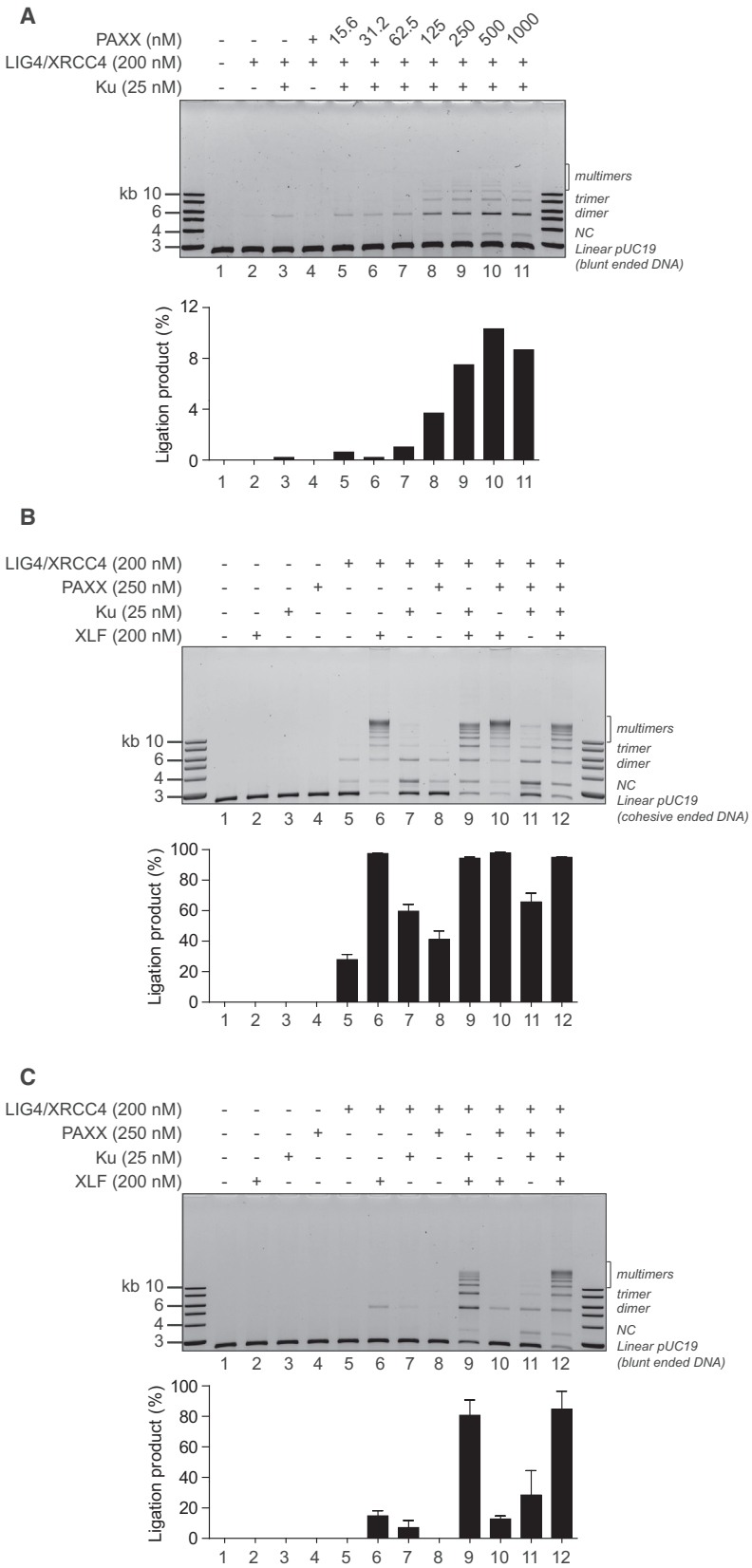

Figure 4. Ku-Dependent Stimulation of LIG4/XRCC4 by PAXX Is Modest Compared to XLF

(A) Ku-dependent stimulation of LIG4/XRCC4 blunt-ended DNA ligation by PAXX titration is shown.

(B and C) Cohesive- (B) and blunt-ended (C) DNA-ligation assays showing that the strongest and major stimulation of Ku-dependent LIG4/XRCC4 is conferred by XLF. Data were quantified from three independent experiments where error bars are indicated (± SEM).

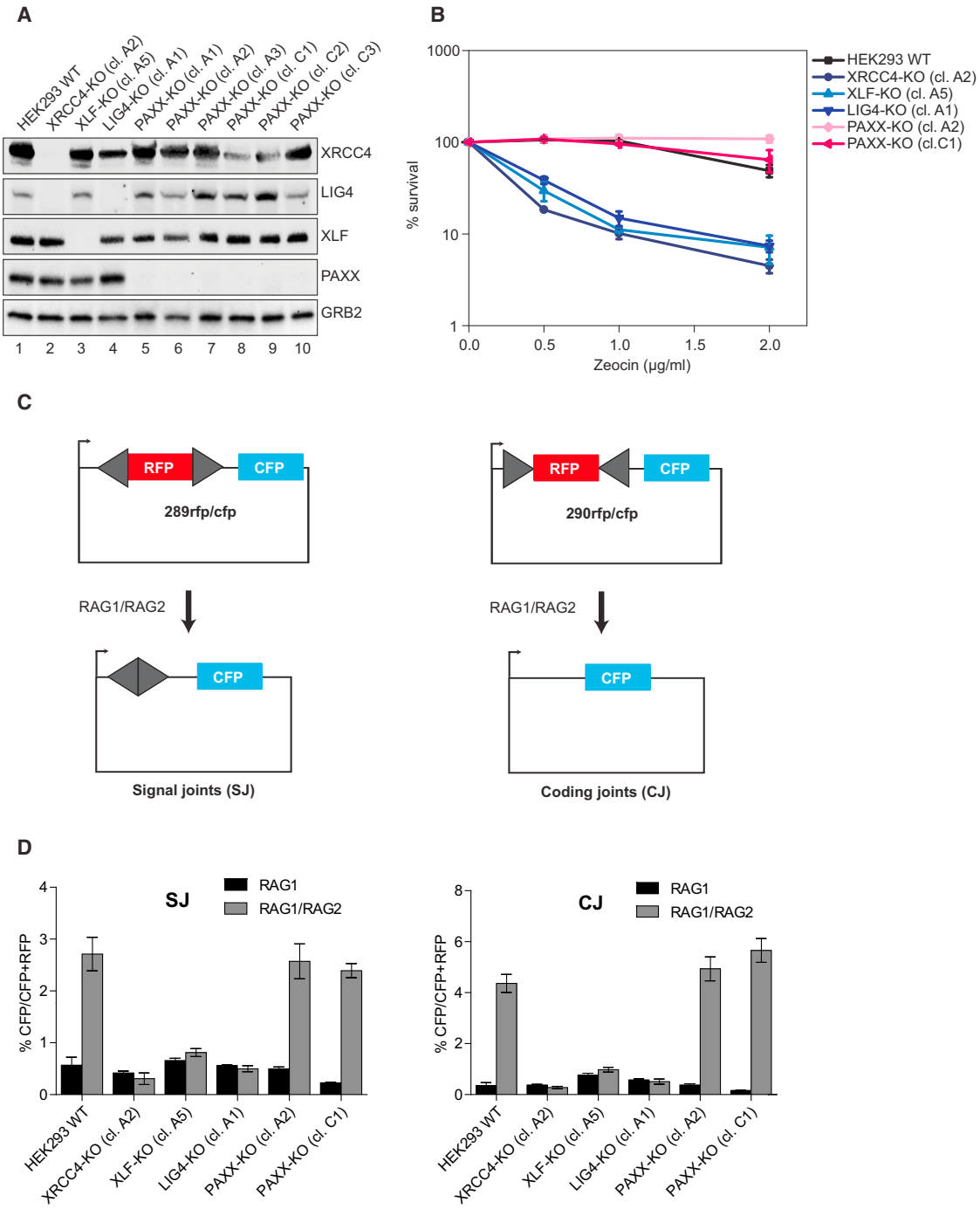

Figure 5. PAXX Is Dispensable for NHEJ in Human Cells

(A) Immunoblotting confirming the absence of XRCC4, XLF, LIG4, and PAXX protein expression in HEK293 CRISPR-Cas9-generated knockout lines. GRB2 is used as an internal loading control. cl. x indicates clone number.

(B) Zeocin sensitivity assays with HEK293 wild-type, XRCC4, XLF, LIG4, and PAXX CRISPR-Cas9-generated knockout lines using CellTiter-Glo are shown.

(C) Episomal fluorescent reporter substrates were utilized to detect signal and coding joints in transient V(D)J assays in HEK293 cells (Neal et al., 2016).

(D) Signal joint (left panel) and coding joint (right panel) efficiencies in XRCC4, XLF, LIG4, and PAXX knockout HEK293 lines. Error bars indicate mean (± SEM) from three independent experiments.

ends (Figure 5D). In contrast, PAXX-deficient HEK293 cells joined both coding and signal ends similarly to wild-type HEK293 cells (Figure 5D). We have shown previously that different human cell strains vary dramatically in their dependence on XLF for efficient c-NHEJ (Roy et al., 2015). Thus, the PAXX gene also was disrupted from the human colorectal tumor cell strain HCT116. As can be seen, HCT116 cells deficient in PAXX had similar sensitivity to Zeocin as wild-type control cells (Figure S5A). Moreover, PAXX-deficient HCT116 cells supported similar levels of V(D)J coding joining as wild-type controls (Figure S5B). We conclude that PAXX is not essential for V(D)J joining; these data are consistent with PAXX functioning as an accessory factor rather than a core c-NHEJ factor.

PAXX Deficiency Accentuates the NHEJ-Defective Phenotype of XLF-Deficient Cells, but Not of DNA-PKcs-Deficient Cells

Recently, we reported that it is XLF's ability to form DNA-tethering filaments with XRCC4 that explains XLF's functional redundancy with ATM (Roy et al., 2015; Zha et al., 2011). Moreover, XLF's ability to stimulate LIG4 is separable from its ability to tether DNA ends as a filament with XRCC4 (Roy et al., 2015). In this study, we investigated the effect of PAXX/XLF ablation, and we concluded that, although PAXX deficiency enhanced the c-NHEJ phenotype of XLF-deficient cells, this was not because of defective filament formation. The observation that the ability of PAXX to stimulate end joining in a Ku-dependent fashion is largely masked by XLF now provides a sound explanation for enhanced deficits in c-NHEJ observed when PAXX is disrupted in XLF-deficient cells.

To further investigate this effect, the neocarzinostatin sensitivity of the HEK293T cells lacking XLF or both XLF and PAXX that we described previously (Roy et al., 2015) was ascertained. As can be seen (Figure S5C), HEK293T cells lacking both XLF and PAXX were more sensitive to neocarzinostatin than cells deficient in XLF alone. Consistent with the Zeocin sensitivity results, PAXX-deficient HEK293T cells were not hypersensitive to neocarzinostatin. The masking of PAXX's ability to stimulate end joining in vitro by XLF would predict that disrupting PAXX in other c-NHEJ-deficient cells would not have the same effect. To that end, PAXX was disrupted in the CHO cell strain V3 that lacks DNA-PKcs. Disruption of PAXX was ascertained by PCR; three clones were selected for study that contained no wild-type PAXX alleles. Sequence analysis of amplified deletions confirmed three unique deletions in each of the three clones selected for study (S.R., unpublished data). V3 cells were hypersensitive to Zeocin because of their deficiency in DNA-PKcs. This sensitivity was reversed by stable expression of DNA-PKcs (Figure S5D). As can be seen, disruption of PAXX in DNA-PKcs-deficient V3 cells did not affect cellular sensitivity to Zeocin (Figure S5D). In sum these data are consistent with PAXX providing a backup mechanism to stimulate LIG4/XRCC4 in the absence of XLF in a Ku-dependent manner.

GFP-PAXX Interactome Includes Both c-NHEJ and a-NHEJ Components

Since PAXX-deficient cells do not display a phenotype consistent with defective c-NHEJ, we considered that PAXX might affect some other cellular process, and we interrogated the PAXX interactome. An N-terminal GFP tag was engineered into PAXX expression plasmids, and the fusion protein was transiently overexpressed in HEK293 cells followed by treatment with calicheamicin-γ1 (Cali) to induce DSBs (Elmroth et al., 2003; Mårtensson et al., 2003). Complexes were recovered using nanobodies directed against the GFP moiety covalently linked to magnetic beads (Figure S1). As can be seen, endogenous Ku70 and Ku80 were efficiently and specifically recovered with GFP-PAXX as well as DNA-PKcs, PARP1, and LIG3 (Figures S1A and S1B). No major differences between Cali-treated and untreated samples were detected except for the phosphorylation of residue S2056 in DNA-PKcs, which indicates that the cells responded to the Cali treatment. Strikingly, we observed that PARP1 was completely polyADP-ribosylated (Figure S1A, right panel anti-PAR); we are currently investigating the basis for this observation. The samples were trypsinized and the resulting peptides were separated by liquid chromatography followed by mass spectrometry analysis.

The results are summarized in Table S1, and they confirm the abundance of Ku70, Ku80, DNA-PKcs, PARP1, LIG3, and even XRCC1 recovered with GFP-PAXX. The results also revealed phosphorylated residues in PAXX that likely included residues S134, T145, S148, and S152, which were not dependent on the Cali treatment (ProteomeXchange: PXD004659). In addition, the identities of the major proteins co-purifying with GFP-PAXX detected by silver staining were further validated by in-gel trypsin digestion followed by mass spectrometry, as indicated accordingly in Figure S1B. The importance of the PAXX C-terminal tails for complex formation with Ku and PARP1 was confirmed by pull-down experiments using GFP-tagged variants of PAXX (Figure S1C). Thus, under the overexpression conditions used here, GFP-PAXX associates with both c-NHEJ and a-NHEJ factors, along with chromatin and DNA damage response factors such as histones and MDC1.

To assess whether PAXX-containing complexes assemble in a DNA-dependent manner, purifications were performed in the presence of ethidium bromide (EtBr) or benzonase. As can be seen, EtBr and benzonase treatments abrogated the interaction between PAXX and Ku70, Ku80, PARP1, and LIG3 (Figure S1D). We conclude that the association of GFP-PAXX with both c-NHEJ and a-NHEJ factors is largely DNA dependent.

The Balance between c-NHEJ and a-NHEJ Is Normal in PAXX-Ablated Cells

A hallmark of c-NHEJ deficiency includes dependence on a-NHEJ for end joining, which is accompanied by increased utilization of micro-homology-mediated end joining (MMEJ; Fattah et al., 2014; Verkaik et al., 2002). Since, GFP-PAXX associates with two putative a-NHEJ components (PARP1 and LIG3), we next considered whether PAXX is involved in controlling the balance between c-NHEJ and a-NHEJ. A plasmid assay that measures the relative contribution of direct end joining versus MMEJ was used (Figure 6A; Oh et al., 2013; Verkaik et al., 2002). The substrate plasmid was predominately joined directly (without use of micro-homology) in wild-type HEK293 cells (Figures 6B, top panel, lanes 1 and 2, and 6C), consistent with c-NHEJ predominating during end joining in human somatic

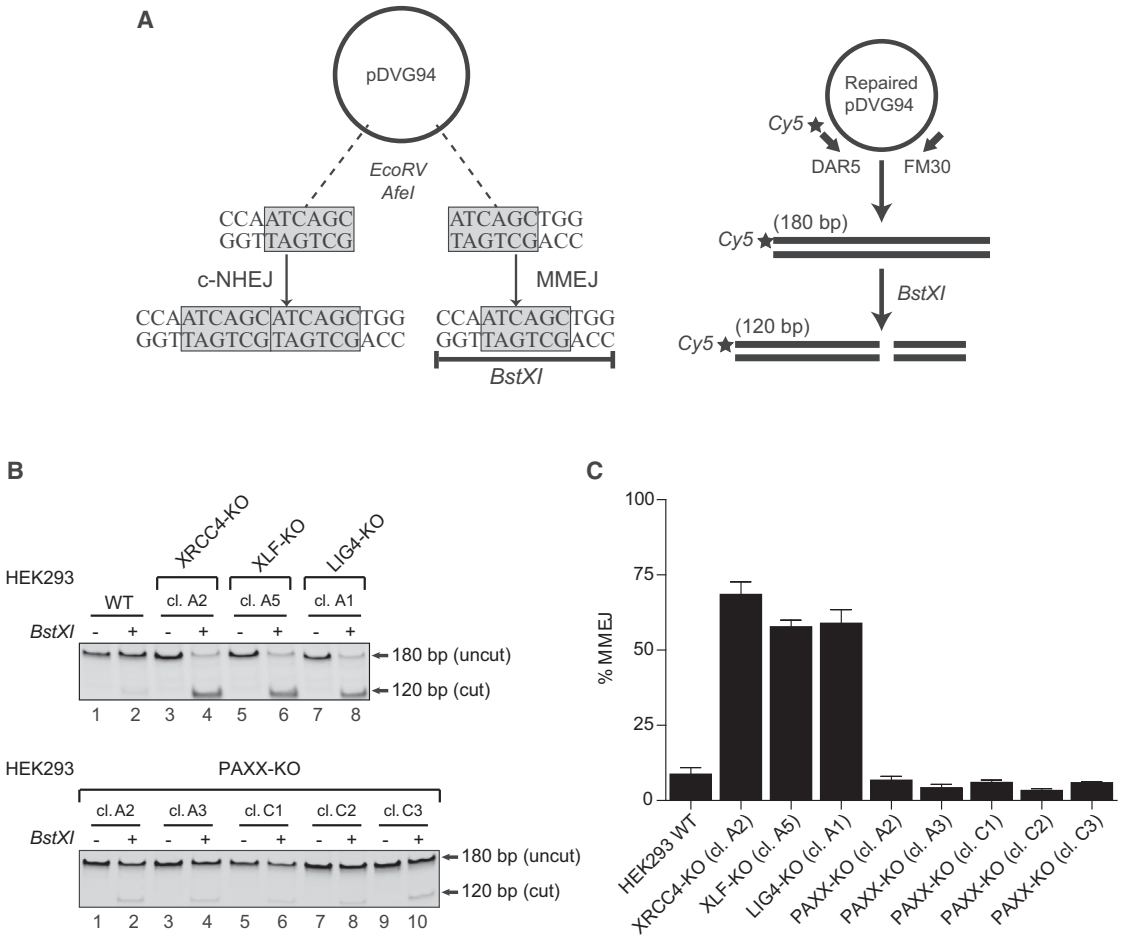

Figure 6. The Balance between c-NHEJ and a-NHEJ Is Normal in PAXX-Ablated Cells

(A) MMEJ reporter assay to detect relative direct ligation versus MMEJ in cells (Verkaik et al., 2002; Oh et al., 2013). After *EcoRV* and *AfeI* restriction enzyme digestion, the reporter substrate pDVG94 becomes a blunt-ended linear plasmid with 6-bp direct repeats at both ends. Repair via c-NHEJ generally retains at least part of either repeat, whereas MMEJ generates only a single repeat and a *BstXI* restriction enzyme site. After transfection of the linearized plasmid, the repaired junctions are analyzed by amplifying a 180-bp fragment with primers flanking the ends and with one of the primers labeled with Cy5, followed by digestion with *BstXI*. The 180-bp fragment resistant to *BstXI* represents repair via c-NHEJ, whereas the 120-bp digestion product represents MMEJ repair.

(B) Wild-type HEK293 cells mostly perform direct repair, while XRCC4, XLF, and LIG4 knockout cell lines show increased repair by MMEJ (top panel). PAXX knockout cell lines (five independent clones, cl. x) mostly perform direct repair as in wild-type cells (bottom panel).

(C) Quantification of the data in (B) from three independent experiments shows the mean (± SEM).

cells. As expected, cells deficient in core c-NHEJ factors (XRCC4, XLF, and LIG4) relied strongly on a-NHEJ, and a strong shift in the use of micro-homology was observed (Figures 6B, top panel, lanes 3–8, and 6C). Remarkably, PAXX-deficient cells rejoined the plasmid substrate completely analogously to wild-type control cells (Figures 6B, bottom panel, and 6C). These data reinforce the conclusion that PAXX is not a core c-NHEJ factor, and they further reinforce the model that PAXX would act as backup for XLF or even for Ku80 deficiencies through its interaction with Ku70 homodimers.

DISCUSSION

The first three studies reporting the identification of PAXX concluded that the protein is a core component involved in DSB repair by c-NHEJ (Craxton et al., 2015; Ochi et al., 2015; Xing et al., 2015). Our data do not support this conclusion and instead suggest that PAXX functions as an accessory factor during c-NHEJ. It thus appears that our findings are in contradiction with the earlier studies. However, careful examination of the clonogenic survival data obtained by analyzing asynchronous PAXX-null chicken DT40 cells or HCT116 cells shows that these cells, in contrast to XRCC4-, XLF-, or LIG4-null cells, are not overtly sensitive to ionizing radiation or to various DSB-inducing agents (Xing et al., 2015). However, when these PAXX-null DT40 cells are arrested in G1/S phase before treatment, their sensitivity to ionizing radiation becomes more pronounced, but not as dramatically hypersensitive as XRCC4-, XLF-, or LIG4-null cells. The function of PAXX might therefore be cell-cycle-phase specific, with a prominent role in G1. Furthermore, based on

genetic epistatic interaction analysis between PAXX- and XLF-null mutations, the study suggested that PAXX and XLF could function together or not, depending on the type of DNA lesions.

In an independent study, clonogenic survival assays after ionizing radiation treatment also were performed in asynchronous HEK293 and U2OS cells downregulated for PAXX via small interfering RNA (siRNA), and the cells displayed mild sensitivity compared to wild-type control cells (Craxton et al., 2015). Surprisingly, XRCC4-depleted cells exhibited a mild sensitivity to ionizing radiation in these experiments, which is unexpected since XRCC4-deficient cells are among the most ionizing radiation-sensitive cells known. Similarly, an siRNA-depletion approach was used to analyze the phenotype of PAXX deficiencies in U2OS cells in a third independent study (Ochi et al., 2015). Again, XRCC4-depleted cells only had a mild phenotype. However, in that study, PAXX-null RPE-1 cells generated by CRISPR-Cas9 genome editing exhibited mild sensitivity to phleomycin, which indicates that the function of PAXX might be more important in primary cells since these hTERT-immortalized RPE-1 cells are believed to behave more like primary cells compared to cancer cells such as U2OS.

We therefore conclude that there are in fact no major discrepancies between our findings and the earlier studies. While our phenotypic analysis of PAXX-null cells, using episomal V(D)J recombination and end joining DNA substrates, may not recapitulate reactions in a chromatin context, overall our data predict that PAXX-deficient mice will not display the severe combined immunodeficiency (SCID) phenotype, associated with c-NHEJ mutations, and will develop a proficient adaptive immune system. Nevertheless, PAXX deficiencies could lead to phenotypes associated with cell-cycle phase or cell-type and differentiation stage.

The PAXX-Ku-DNA Ternary Complex

One important property of PAXX that emerged from previous studies, confirmed and further analyzed here, is its ability to associate with DNA-bound Ku, forming a ternary complex detectable by EMSA (Ochi et al., 2015; Xing et al., 2015). Understanding the organization and dynamics of PAXX-Ku-DNA ternary complexes will be important to unravel functionally relevant roles of PAXX. The protein-protein contacts involved in the ternary complex are not yet defined. A PAXX homodimer could interact directly with Ku70, Ku80, or both subunits of the Ku heterodimer. Here we report that PAXX can form a ternary complex with DNA-bound Ku70 (Figure 3), suggesting a protein-protein contact between Ku70 and PAXX. Two Ku-binding motifs (KBMs) have been defined recently as APLF-like or XLF-like (Grundy et al., 2016). The APLF-like KBM directly interacts with a hydrophobic pocket in the von Willebrand factor A domain of Ku80 (Grundy et al., 2013; Shirodkar et al., 2013). In contrast, mapping of the interaction site on Ku of the XLF-like KBM has not been determined. Interestingly, our ITC analysis revealed that PAXX interacts with DNA-bound Ku with ~4 μM K_d, while the XLF interaction with DNA-bound Ku is much stronger with a measured ~20 nM K_d in the same experimental conditions (C.N., unpublished data). A previous study reported a tighter binding of PAXX with Ku-DNA (K_d of 14.5 nM), with the interaction measured by surface plasmon resonance (SPR) and with a 107-bp DNA bound by biotin tag (Ochi et al., 2015). The crystal structures of Ku-DNA complexes with XLF or PAXX motifs or proteins will provide a more complete understanding of how Ku orients these factors adjacent to the actual DSB.

Another major issue concerns the stoichiometry of the PAXX-Ku-DNA ternary complex. One PAXX homodimer could simply bind a single DNA-bound Ku heterodimer or perhaps bridge two Ku heterodimers bound to two independent DNA molecules to favor ligation, as proposed before (Ochi et al., 2015). Other possibilities such as one PAXX homodimer interacting with two Ku heterodimers bound to the same DNA or even two PAXX homodimers interacting with one Ku heterodimer could be involved as well. Regardless of the stoichiometry, the stability of the PAXX-Ku-DNA complex is strictly DNA dependent (Craxton et al., 2015; Xing et al., 2015; Figures 1, 2, and 3; Figure S1; Table 1). While the interaction of PAXX with DNA in the absence of Ku is undetectable, as well as the direct interaction between PAXX and Ku in solution, we reveal here that PAXX-Ku interaction not only requires Ku to be loaded onto DNA but also is stabilized by a bare DNA extension, single or double stranded.

Two models could be proposed for PAXX-Ku-DNA ternary complex organization. Either PAXX contacts Ku and DNA at the same time in the complex, or PAXX never contacts DNA directly but interacts with Ku only when the latter is loaded onto DNA. This second model would then involve a change in conformation of Ku upon DNA binding. Conformational changes between the crystal structures of Ku free or bound to DNA are noticeable (Walker et al., 2001). For example, residue W148 in the von Willebrand factor A domain of Ku70 protrudes out more prominently on the surface of DNA-bound Ku and could be part of the PAXX or XLF interaction interface. Interestingly, this position is conserved in Ku70 alignment and is the equivalent position of Ku80 I112 that is involved in APLF binding (Grundy et al., 2013). Such a scenario would allow PAXX to contact Ku only when the latter is threaded onto DNA but without directly contacting DNA by itself. Yet our analysis shows that ~15 bp or nt of bare DNA extension stabilizes the PAXX-Ku-DNA ternary complex (Figure 2). What would be the role of this DNA extension in complex stabilization? PAXX could directly interact with the bare DNA extension after binding to DNA-bound Ku, and, as reported for DNA-PKcs, it could push end-bound Ku inward (Yoo and Dynan, 1999). Alternatively, the bare DNA extension could instead induce a conformational change in DNA-bound Ku. One attractive idea is that PAXX binding to DNA-bound Ku would trigger interaction of the C-terminal region of Ku70 containing the SAP domain and/or the C-terminal region of Ku80 with the bare DNA extension. It should be stressed that both Ku70 and Ku80 C-terminal domains are missing in the reported crystal structures and that we have therefore only a partial view of the actual structural organization of Ku when threaded onto DNA (Walker et al., 2001).

Further, we tested here whether saturating amounts of PAXX could lock Ku on DNA ends and prevent threading of multiple Ku units onto a large 1.1-kb DNA fragment and long-distance translocation, but we found no major effect of PAXX (Figure 2H). Instead of slowing Ku translocation and locking it at or close to a DNA end, PAXX might accelerate Ku diffusion on DNA, and, in that case, kinetics experiments would be required to test this possibility.

The Effect of PAXX on LIG4/XRCC4 Activity

The previously reported Ku-dependent stimulation of LIG4/XRCC4 by PAXX is reproduced here using direct ligation assays that include Ku, XLF, PAXX, and LIG4/XRCC4 (Ochi et al., 2015; Xing et al., 2015; Figure 4). We find that the Ku-dependent stimulation of LIG4/XRCC4 by PAXX is relatively weak and that the full extent of this PAXX stimulation is uncovered if XLF is omitted in the ligation reaction, especially in the case of blunt-end ligation (Figure 4C). We deduce from this analysis that PAXX might indeed promote end-end bridging with Ku to favor ligation as proposed earlier (Ochi et al., 2015). However, consistent with our previous study, PAXX/XLF double-deficient cells exhibit greater Zeocin sensitivity compared to XLF-deficient cells, while PAXX-deficient cells show no sensitivity (Roy et al., 2015). It appears that stimulation of LIG4/XRCC4 is dominantly supported by XLF in a Ku-dependent manner. Assuming XLF somehow prevents PAXX from accessing its interaction site with Ku70 either by direct competition or by an overall steric hindrance, the ~100-fold higher affinity of XLF for DNA-bound Ku discussed above could be an explanation for XLF's ability to mask PAXX's role in Ku-dependent LIG4/XRCC4 stimulation by XLF.

Other Potential Roles and Regulation of PAXX

The role of PAXX in c-NHEJ is thus minor and might be critical only in special circumstances when assistance is needed for stabilization of complex end-end interactions (Ochi et al., 2015; Xing et al., 2015). Alternatively, PAXX could be important at the level of the chromatin substrate or the DNA damage response. Indeed, we find in our PAXX interactome abundant recovery of histones and chromatin remodelers as well as the MDC1 DNA damage response protein (Table S1). Equally untested is whether PAXX could influence the 5′-dRP/AP lyase activity of Ku at or near broken DNA ends or the other activities of Ku70 or Ku80 not related to c-NHEJ (Roberts et al., 2010). Finally, we show here that PAXX could be subject to post-translational modification by phosphorylation on residues S134, T145, S148, and S152. Phospho-mimicry of these modifications by substitutions to aspartate residues destabilizes the PAXX-Ku-DNA ternary complex as measured by EMSA (Figure 3D), but does not affect its stimulation of LIG4/XRCC4 blunt-ended DNA-ligation activity (Figures S4B and S4D). The functional relevance of these PAXX phosphorylations remains thus unknown and will require further analysis to reveal their roles.

To conclude, PAXX appears to play an accessory role during c-NHEJ that is largely overlapped by XLF. PAXX's function might take part in a backup mechanism when XLF is defective or, for example, sequestrated in the cytoplasm via Akt phosphorylation (Liu et al., 2015). Given the functional redundancy between XLF and ATM (Zha et al., 2011), it would be informative to analyze PAXX/ATM double-deficient and PAXX/ATM/XLF triple-deficient cells to reveal overlays between backup mechanisms during c-NHEJ. Finally, the interaction of PAXX with Ku70 homodimers and its first functional role described in this study re-open the question of the role of the Ku70 homodimer in DNA repair or metabolism and potentially in other cellular processes. However, there is currently no clear evidence that a fraction of Ku70 exists as a homodimer in cells. Intracellular levels of Ku70 homodimers will likely be very low since normal steady-state levels depend on the presence of Ku80.

EXPERIMENTAL PROCEDURES

Plasmid Constructs and Protein Purification

Recombinant XLF and LIG4/XRCC4 complexes were obtained using constructs and procedures described previously (Andres et al., 2007; Wu et al., 2009). Ku and Ku70 were expressed in insect cells and purified as described (Ono et al., 1994), as well as the truncated Ku_{cc} heterodimer that includes residues 1–544 of Ku70 and N-terminally poly-histidine-tagged residues 1–551 of Ku80. The Ku and Ku70 preparations were analyzed by analytical size exclusion chromatography to verify assembly of Ku heterodimers and Ku70 homodimers, respectively (Figure S6). Full-length Ku70, C-terminally tagged with six histidines, was produced in bacteria using a construct pMM1271 obtained by cloning the Ku70 cDNA with a C-terminal poly-histidine tag in between the *NdeI* and *XhoI* sites of pETduet-1 (Novagen). Ku70 purification from bacteria was performed as described (Hanakahi, 2007).

The PAXX (C9orf142) expression construct was generated by PCR amplification using cDNA clone MGC:2999 IMAGE clone 3161564 as template, engineering an *NcoI* restriction enzyme site at the ATG and an *XhoI* site after the STOP codon and first cloned into pCR-Blunt (Thermo Fisher Scientific). The insert was released with *NcoI-XhoI* and subcloned into the *NcoI-XhoI* sites of pHIS parallel-I (Sheffield et al., 1999). Similarly, the PAXX open reading frame (ORF) was PCR amplified adding EcoRI-*BamHI* sites for subcloning into EcoRI-*BglII* of pEGFP-C2 (Clontech Laboratories). The pHIS parallel-I vector carrying the $PAXX^{1–204}$ ORF was used for site-directed mutagenesis (Q5, New England Biolabs, oligonucleotides listed in Table S3) to produce $PAXX^{\Delta C1}$, $PAXX^{\Delta C2}$, $PAXX^{3R}$, $PAXX^{3K}$, $PAXX^{ALA}$, and $PAXX^{ASP}$. The coding regions of wild-type PAXX and variants $PAXX^{\Delta C1}$, $PAXX^{\Delta C2}$, $PAXX^{3R}$, $PAXX^{3K}$, $PAXX^{ALA}$, and $PAXX^{ASP}$ were PCR amplified adding terminal EcoRI-*BamHI* sites and subcloned into EcoRI-*BglII* sites of pEGFP-C2 mammalian expression vector (Clontech Laboratories). All plasmid constructs were verified by DNA sequencing and are listed in Table S4. PAXX derivatives were produced in *Escherichia coli* Rosetta/pLysS cells and purified by immobilized Ni^{2+} ion affinity chromatography (GE Healthcare), followed by Sepharose Q chromatography as described previously (Roy et al., 2015).

Purified proteins were dialyzed in 20 mM Tris-HCl (pH 8.0), 150 mM NaCl, 1 mM DTT, 1 mM EDTA, and 10% glycerol and stored at −80°C. Protein concentrations are expressed in molarity of monomers for PAXX and XLF, of heterodimers for Ku, of homodimers for Ku70, and of 1:2 complexes for LIG4/XRCC4.

EMSA

Binding reactions (10 μL) were performed by incubating the annealed oligonucleotides (oligonucleotides used in this study are listed in Table S3 and indicated in the figure legends) at a final concentration of 25 nM, with the indicated final concentrations of proteins in 75 mM KCl, 10 mM Tris (pH 7.5), 0.5 mM EDTA, 0.5 mM DTT, 0.5 mg/mL acetylated-BSA, and 5% glycerol. Reactions were incubated at room temperature for 1 hr and fractionated by 6% PAGE (29%/1% [w/v] Acrylamide:Bis-acrylamide) in 0.5× standard Tris-borate-EDTA (TBE) buffer at 80 V for 45 min to 1 hr. After electrophoresis, DNA was visualized using a ChemiDoc MP imaging system (Bio-Rad), either by direct detection of the fluorescently labeled DNA (FAM) or after staining with 0.2 μg/mL EtBr. Data were processed and quantified with the Image Lab software version 5.2.1 (Bio-Rad). The DNA-binding assays with the *BglI* fragment of pUC19 (1.1 kb) used at 5 ng/μl were incubated similarly and fractionated by 0.8% w/v agarose gel electrophoresis in 0.5× standard TBE buffer at 80 V for 1 hr. DNA was stained with 0.2 μg/mL EtBr and analyzed as indicated above.

ITC Experiments

Interaction with the different Ku or Ku70 constructs, free or in the presence of the various DNA substrates, was determined using a VP-ITC calorimeter (Microcal). Prior to measurements, all solutions were degassed under vacuum. The reaction cell (1.8 mL) was loaded with between 6 and 12 μM Ku or Ku70 solutions. The syringe (500 μL) was filled with PAXX protein or peptide at

concentrations between 100 and 180 μM. The proteins were extensively dialyzed against the same buffer (20 mM Tris [pH 8.0], 150 mM NaCl, and 5 mM β-mercaptoethanol). Control experiments were performed with protein and peptide solutions injected into buffer or without Ku or without DNA in the reaction cell. Thermodynamic parameters ΔH, N, and Ka were obtained by nonlinear least-squares fitting of the experimental data using the single set of independent binding sites model of the Origin software provided with the instrument. The free energy of binding (ΔG) and the entropy (ΔS) were determined using the classical thermodynamic formulas, $\Delta G = -RT\ \ln(Ka)$ and $\Delta G = \Delta H - T\Delta S$. All binding experiments were performed in duplicate or triplicate at 25°C.

DNA-Ligation Assays

Reaction mixtures (10 μL) contained 50 ng linearized pUC19 plasmid (digested with *XbaI* for cohesive-end ligation or with SmaI for blunt-end ligation), 75 mM KCl, 2 mM $MgCl_2$, 1 mM ATP, 10 mM HEPES (pH 8.0), 0.5 mM EDTA, 0.5 mM DTT, 5% glycerol, and the indicated final concentrations of proteins. Following a 1-hr incubation at room temperature, the samples were deproteinized by the addition of pronase (1.25 μg/μL final concentration) and Sarkosyl (1.25% final concentration) and incubated at 55°C for 30 min. The reaction mixtures were fractionated by 0.8% (w/v) agarose gel electrophoresis in 1× standard TBE buffer at 80 V for 2 hr followed by EtBr staining. Gel images were acquired and quantified as indicated for the EMSAs.

Cell Culture

HEK293 and HCT116 cells were cultured in DMEM supplemented with 10% fetal bovine serum, 100 U/mL penicillin, and 100 μg/mL streptomycin (all reagents from Life Technologies). V3 cells were cultured in minimal essential media supplemented with 10% newborn calf serum, 100 U/mL penicillin, and 100 μg/mL streptomycin (all reagents from Life Technologies). Cells were maintained at 37°C with 5% CO_2. Zeocin sensitivity assays with HEK293 wild-type, XRCC4, XLF, LIG4, and PAXX CRISPR-Cas9-generated knockout lines were assayed using CellTiter-Glo as recommended by the manufacturer (Promega).

Anti-GFP Pull-Down and Mass Spectrometry Analysis

HEK293 cells (10-cm dish, 80% confluent) were transfected with 15 μg plasmid DNA expressing wild-type GFP-PAXX or variants, pre-incubated with 30 μl polyethyleneimine solution (PEI) at 1 mg/mL made in H_2O and buffered at pH 7.2 with HCl (Polysciences). After 24 hr, the cells were harvested and the pellets were directly extracted for 30 min with buffer A (20 mM Tris-HCl [pH 7.5], 300 mM NaCl, 1 mM Na_3VO_4, 1 mM NaF, 1% NP40, 1 mM PMSF, and 10% glycerol supplemented with complete EDTA-free protease inhibitor cocktail [Roche]). After incubation, 1 vol of buffer B (20 mM Tris-HCl [pH 7.5], 1 mM Na_3VO_4, 1 mM NaF, 1% NP40, 1 mM PMSF, 10% glycerol, and complete EDTA-free protease inhibitor cocktail) was added. Following ultra-centrifugation at 14,000 rpm for 30 min at 4°C, the supernatant was incubated with anti-GFP nanobodies coupled to magnetic beads, prepared as described (Meek et al., 2012), with end-to-end mixing for 16 hr at 4°C. For exposure to DNA-damaging agents, cells were exposed to freshly diluted Cali (4 nM) in medium for 1 hr and then harvested as described (Cheng et al., 2011). In some experiments, EtBr (50 μg/mL) or benzonase (25 units/mL, Novagen) was added in the extraction buffer. Bound complexes were washed at least three times (10 min) with buffer A + B (1:1 v/v). Finally, beads with the bound complexes were directly re-suspended in SDS loading buffer (50 mM Tris-HCl [pH 6.8], 2% SDS, 300 mM 2-mercaptoethanol, 0.01% bromophenol blue, and 10% glycerol), fractionated by reducing and denaturing SDS-PAGE, and analyzed by Coomassie or silver staining and mass spectrometry.

The mass spectrometry procedures and data analysis are described in the Supplemental Experimental Procedures.

Antibodies

Antibodies used for immunoblotting include rabbit polyclonal anti-DNA-PKcs-phospho-S2056 (Abcam, ab18192), rabbit polyclonal anti-PARP (Novus Biologicals, NBP2-13732), rabbit polyclonal anti-PARP (Novus Biologicals, NBP2-13732), rabbit polyclonal anti-PAR (Trevigen, 4336-BPC-100), rabbit polyclonal anti-LIG3 (Novus Biologicals, NBP1-87720), rabbit monoclonal anti-Ku80 (Abcam, ab80592), rabbit monoclonal anti-Ku70 (Abcam, ab92450), goat polyclonal anti-C9orf142 for PAXX (Santa Cruz Biotechnology, sc-245999), rabbit polyclonal NIH13 anti-XRCC4 (Modesti et al., 1999), goat polyclonal anti-XLF (Novus Biologicals, NB100-53799), rabbit polyclonal anti-LIG4 (Abcam, ab80514), and mouse monoclonal anti-GRB2 (BD Biosciences, 610111). All the antibodies were used at the dilution of 1:2,000.

Generation of HEK293 Knockout Cells

Cas9-targeted gene disruption was performed using methods similar to those reported previously (Ran et al., 2013). Oligonucleotides used to generate derivatives of pSpCas9(BB)-2A-GFP (Addgene plasmid 48138) expressing guide RNAs (gRNAs) targeting PAXX, XRCC4, XLF, and LIG4 genes are listed in Table S5. Then 2 days after transfection with the targeting vectors using PEI as transfection reagent, HEK293 cells were sorted based on GFP expression and isolated single cells were amplified. Clones were screened by immunoblotting, followed by genotyping by PCR amplification of the targeted locus from genomic DNA (primers listed in Table S5), and analyzed by DNA sequencing.

Transient V(D)J Recombination Assays

Transient V(D)J recombination assays utilizing the signal joint (289 red fluorescent protein (RFP)/CFP) and coding joint substrates (290 RFP/CFP) were performed as described previously (Neal et al., 2016). Briefly, 5×10^4 HEK293 cells were seeded into 6-cm dishes, grown for 1 day to 40%–60% confluence, and transfected with 1 μg substrate-, 2 μg RAG1-, and 2 μg RAG2-expressing plasmids per well using PEI as transfection reagent (2 μg PEI/1 μg plasmid). Cells were harvested 48 hr after transfection and analyzed for CFP and RFP expression by flow cytometry. Recombination frequencies were calculated as the ratio of cells that were double positive for RFP and CFP fluorescence over total cells that were only positive for RFP fluorescence. Experiments were performed in triplicate.

MMEJ Assays

Assays were performed as described previously (Fattah et al., 2014; Oh et al., 2013; Verkaik et al., 2002). Briefly, 5×10^4 cells were seeded into 6-cm plates and transfected with plasmid pDVG94 linearized with *EcoRV* and *AfeI* (1 μg/2 μg PEI). Plasmid DNA was recovered using the Hirt extraction method (Hirt, 1967) 48 hr after transfection. Junctions were PCR amplified using primers FM30 and Cy5-labeled DAR5 (Table S3). PCR products were then digested with *BstXI* and the products were separated by electrophoresis on a 4%–20% polyacrylamide gel using 0.5× standard TBE buffer at 80 V for 3 hr. Fluorescent signal was detected with a Chemidoc MP imaging system (Bio-Rad), and the bands representing the undigested (180-bp) or digested (120-bp) PCR products were quantified using ImageJ software version 1.48. Experiments were performed in triplicate.

ACCESSION NUMBERS

The accession number for the mass spectrometry proteomics data reported in this paper is ProteomeXchange: PXD004659 (Vizcaíno et al., 2016). Included are tables of GFP-PAXX pull-down raw data; GFP-PAXX pull-down raw data, peptide-spectrum match only; and PAXX phosphorylation raw data.

SUPPLEMENTAL INFORMATION

Supplemental Information includes Supplemental Experimental Procedures, six figures, and five tables and can be found with this article online at http://dx.doi.org/10.1016/j.celrep.2016.09.026.

AUTHOR CONTRIBUTIONS

Conceptualization, S.K.T. and M.M.; Investigation, S.K.T., C.T.-L., C.N., P.D., S.R., and S.A.; Writing – Original Draft, S.K.T. and M.M.; Writing – Review & Editing, S.K.T., J.-B.C., K.M., and M.M.; Funding Acquisition, J.-B.C., K.M., and M.M.; Supervision, J.-B.C., K.M., and M.M.

ACKNOWLEDGMENTS

We thank Emilie Baudelet from the Cancer Research Center of Marseille (CRCM) proteomics and mass spectrometry platform, Marie-Laure Thibult and Françoise Mallet from the CRCM cytometry platform, and Audrey Restouin and Rémy Castellano from the CRCM TrGET preclinical assay platform. This work was supported by Public Health Service grant AI048758 (K.M.), grant PLBIO13-099 from the French National Cancer Institute (M.M.), the ARC Foundation for Cancer Research (M.M.), and ANR-12-BSV8-0012 ARC program SLS220120605310 and FRISBI infrastructure ANR-10-INSB-05 (J.-B.C.). The core facility of Marseille Proteomics was supported by Infrastructures Biologie Santé et Agronomie (IBISA), Cancéropôle PACA, Provence-Alpes-Côte d'Azur Region.

Received: August 9, 2016
Revised: August 31, 2016
Accepted: September 9, 2016
Published: October 4, 2016

REFERENCES

Akopiants, K., Zhou, R.-Z., Mohapatra, S., Valerie, K., Lees-Miller, S.P., Lee, K.-J., Chen, D.J., Revy, P., de Villartay, J.-P., and Povirk, L.F. (2009). Requirement for XLF/Cernunnos in alignment-based gap filling by DNA polymerases lambda and mu for nonhomologous end joining in human whole-cell extracts. Nucleic Acids Res. *37*, 4055–4062.

Allaway, G.P., Vivino, A.A., Kohn, L.D., Notkins, A.L., and Prabhakar, B.S. (1990). Characterization of the 70KDA component of the human Ku autoantigen expressed in insect cell nuclei using a recombinant baculovirus vector. Biochem. Biophys. Res. Commun. *168*, 747–755.

Andres, S.N., Modesti, M., Tsai, C.J., Chu, G., and Junop, M.S. (2007). Crystal structure of human XLF: a twist in nonhomologous DNA end-joining. Mol. Cell *28*, 1093–1101.

Audebert, M., Salles, B., Weinfeld, M., and Calsou, P. (2006). Involvement of polynucleotide kinase in a poly(ADP-ribose) polymerase-1-dependent DNA double-strand breaks rejoining pathway. J. Mol. Biol. *356*, 257–265.

Cheng, Q., Barboule, N., Frit, P., Gomez, D., Bombarde, O., Couderc, B., Ren, G.-S., Salles, B., and Calsou, P. (2011). Ku counteracts mobilization of PARP1 and MRN in chromatin damaged with DNA double-strand breaks. Nucleic Acids Res. *39*, 9605–9619.

Chiruvella, K.K., Liang, Z., and Wilson, T.E. (2013). Repair of double-strand breaks by end joining. Cold Spring Harb. Perspect. Biol. *5*, a012757.

Craxton, A., Somers, J., Munnur, D., Jukes-Jones, R., Cain, K., and Malewicz, M. (2015). XLS (c9orf142) is a new component of mammalian DNA double-stranded break repair. Cell Death Differ. *22*, 890–897.

de Villartay, J.-P. (2015). Congenital defects in V(D)J recombination. Br. Med. Bull. *114*, 157–167.

Deriano, L., and Roth, D.B. (2013). Modernizing the nonhomologous end-joining repertoire: alternative and classical NHEJ share the stage. Annu. Rev. Genet. *47*, 433–455.

Dudley, D.D., Chaudhuri, J., Bassing, C.H., and Alt, F.W. (2005). Mechanism and control of V(D)J recombination versus class switch recombination: similarities and differences. Adv. Immunol. *86*, 43–112.

Elmroth, K., Nygren, J., Mårtensson, S., Ismail, I.H., and Hammarsten, O. (2003). Cleavage of cellular DNA by calicheamicin gamma1. DNA Repair (Amst.) *2*, 363–374.

Fattah, F.J., Kweon, J., Wang, Y., Lee, E.H., Kan, Y., Lichter, N., Weisensel, N., and Hendrickson, E.A. (2014). A role for XLF in DNA repair and recombination in human somatic cells. DNA Repair (Amst.) *15*, 39–53.

Frit, P., Barboule, N., Yuan, Y., Gomez, D., and Calsou, P. (2014). Alternative end-joining pathway(s): bricolage at DNA breaks. DNA Repair (Amst.) *17*, 81–97.

Grundy, G.J., Rulten, S.L., Zeng, Z., Arribas-Bosacoma, R., Iles, N., Manley, K., Oliver, A., and Caldecott, K.W. (2013). APLF promotes the assembly and activity of non-homologous end joining protein complexes. EMBO J. *32*, 112–125.

Grundy, G.J., Rulten, S.L., Arribas-Bosacoma, R., Davidson, K., Kozik, Z., Oliver, A.W., Pearl, L.H., and Caldecott, K.W. (2016). The Ku-binding motif is a conserved module for recruitment and stimulation of non-homologous end-joining proteins. Nat. Commun. *7*, 11242.

Gu, J., Lu, H., Tsai, A.G., Schwarz, K., and Lieber, M.R. (2007). Single-stranded DNA ligation and XLF-stimulated incompatible DNA end ligation by the XRCC4-DNA ligase IV complex: influence of terminal DNA sequence. Nucleic Acids Res. *35*, 5755–5762.

Hanakahi, L.A. (2007). 2-Step purification of the Ku DNA repair protein expressed in Escherichia coli. Protein Expr. Purif. *52*, 139–145.

Hirt, B. (1967). Selective extraction of polyoma DNA from infected mouse cell cultures. J. Mol. Biol. *26*, 365–369.

Lieber, M.R. (2010). The mechanism of double-strand DNA break repair by the nonhomologous DNA end-joining pathway. Annu. Rev. Biochem. *79*, 181–211.

Liu, P., Gan, W., Guo, C., Xie, A., Gao, D., Guo, J., Zhang, J., Willis, N., Su, A., Asara, J.M., et al. (2015). Akt-mediated phosphorylation of XLF impairs non-homologous end-joining DNA repair. Mol. Cell *57*, 648–661.

Mansour, W.Y., Rhein, T., and Dahm-Daphi, J. (2010). The alternative end-joining pathway for repair of DNA double-strand breaks requires PARP1 but is not dependent upon microhomologies. Nucleic Acids Res. *38*, 6065–6077.

Mårtensson, S., Nygren, J., Osheroff, N., and Hammarsten, O. (2003). Activation of the DNA-dependent protein kinase by drug-induced and radiation-induced DNA strand breaks. Radiat. Res. *160*, 291–301.

Meek, K., Lees-Miller, S.P., and Modesti, M. (2012). N-terminal constraint activates the catalytic subunit of the DNA-dependent protein kinase in the absence of DNA or Ku. Nucleic Acids Res. *40*, 2964–2973.

Modesti, M., Hesse, J.E., and Gellert, M. (1999). DNA binding of Xrcc4 protein is associated with V(D)J recombination but not with stimulation of DNA ligase IV activity. EMBO J. *18*, 2008–2018.

Neal, J.A., Xu, Y., Abe, M., Hendrickson, E., and Meek, K. (2016). Restoration of ATM expression in DNA-PKcs-deficient cells inhibits signal end joining. J. Immunol. *196*, 3032–3042.

Nussenzweig, A., and Nussenzweig, M.C. (2007). A backup DNA repair pathway moves to the forefront. Cell *131*, 223–225.

Ochi, T., Blackford, A.N., Coates, J., Jhujh, S., Mehmood, S., Tamura, N., Travers, J., Wu, Q., Draviam, V.M., Robinson, C.V., et al. (2015). DNA repair. PAXX, a paralog of XRCC4 and XLF, interacts with Ku to promote DNA double-strand break repair. Science *347*, 185–188.

Oh, S., Wang, Y., Zimbric, J., and Hendrickson, E.A. (2013). Human LIGIV is synthetically lethal with the loss of Rad54B-dependent recombination and is required for certain chromosome fusion events induced by telomere dysfunction. Nucleic Acids Res. *41*, 1734–1749.

Oh, S., Harvey, A., Zimbric, J., Wang, Y., Nguyen, T., Jackson, P.J., and Hendrickson, E.A. (2014). DNA ligase III and DNA ligase IV carry out genetically distinct forms of end joining in human somatic cells. DNA Repair (Amst.) *21*, 97–110.

Ono, M., Tucker, P.W., and Capra, J.D. (1994). Production and characterization of recombinant human Ku antigen. Nucleic Acids Res. *22*, 3918–3924.

Ouyang, H., Nussenzweig, A., Kurimasa, A., Soares, V.C., Li, X., Cordon-Cardo, C., Li, Wh., Cheong, N., Nussenzweig, M., Iliakis, G., et al. (1997). Ku70 is required for DNA repair but not for T cell antigen receptor gene recombination In vivo. J. Exp. Med. *186*, 921–929.

Ramsden, D.A., and Asagoshi, K. (2012). DNA polymerases in nonhomologous end joining: are there any benefits to standing out from the crowd? Environ. Mol. Mutagen. *53*, 741–751.

Ran, F.A., Hsu, P.D., Wright, J., Agarwala, V., Scott, D.A., and Zhang, F. (2013). Genome engineering using the CRISPR-Cas9 system. Nat. Protoc. *8*, 2281–2308.

Riballo, E., Woodbine, L., Stiff, T., Walker, S.A., Goodarzi, A.A., and Jeggo, P.A. (2009). XLF-Cernunnos promotes DNA ligase IV-XRCC4 re-adenylation following ligation. Nucleic Acids Res. *37*, 482–492.

Roberts, S.A., Strande, N., Burkhalter, M.D., Strom, C., Havener, J.M., Hasty, P., and Ramsden, D.A. (2010). Ku is a 5′-dRP/AP lyase that excises nucleotide damage near broken ends. Nature *464*, 1214–1217.

Roy, S., de Melo, A.J., Xu, Y., Tadi, S.K., Négrel, A., Hendrickson, E., Modesti, M., and Meek, K. (2015). XRCC4/XLF interaction is variably required for DNA repair and is not required for ligase IV stimulation. Mol. Cell. Biol. *35*, 3017–3028.

Sheffield, P., Garrard, S., and Derewenda, Z. (1999). Overcoming expression and purification problems of RhoGDI using a family of "parallel" expression vectors. Protein Expr. Purif. *15*, 34–39.

Shirodkar, P., Fenton, A.L., Meng, L., and Koch, C.A. (2013). Identification and functional characterization of a Ku-binding motif in aprataxin polynucleotide kinase/phosphatase-like factor (APLF). J. Biol. Chem. *288*, 19604–19613.

Tsai, C.J., Kim, S.A., and Chu, G. (2007). Cernunnos/XLF promotes the ligation of mismatched and noncohesive DNA ends. Proc. Natl. Acad. Sci. USA *104*, 7851–7856.

Verkaik, N.S., Esveldt-van Lange, R.E.E., van Heemst, D., Brüggenwirth, H.T., Hoeijmakers, J.H.J., Zdzienicka, M.Z., and van Gent, D.C. (2002). Different types of V(D)J recombination and end-joining defects in DNA double-strand break repair mutant mammalian cells. Eur. J. Immunol. *32*, 701–709.

Vizcaíno, J.A., Csordas, A., del-Toro, N., Dianes, J.A., Griss, J., Lavidas, I., Mayer, G., Perez-Riverol, Y., Reisinger, F., Ternent, T., et al. (2016). 2016 update of the PRIDE database and its related tools. Nucleic Acids Res. *44* (*D1*), D447–D456.

Walker, J.R., Corpina, R.A., and Goldberg, J. (2001). Structure of the Ku heterodimer bound to DNA and its implications for double-strand break repair. Nature *412*, 607–614.

Wang, J., Satoh, M., Chou, C.H., and Reeves, W.H. (1994). Similar DNA binding properties of free P70 (KU) subunit and P70/P80 heterodimer. FEBS Lett. *351*, 219–224.

Wang, J., Dong, X., Myung, K., Hendrickson, E.A., and Reeves, W.H. (1998a). Identification of two domains of the p70 Ku protein mediating dimerization with p80 and DNA binding. J. Biol. Chem. *273*, 842–848.

Wang, J., Dong, X., and Reeves, W.H. (1998b). A model for Ku heterodimer assembly and interaction with DNA. Implications for the function of Ku antigen. J. Biol. Chem. *273*, 31068–31074.

Wang, H., Rosidi, B., Perrault, R., Wang, M., Zhang, L., Windhofer, F., and Iliakis, G. (2005). DNA ligase III as a candidate component of backup pathways of nonhomologous end joining. Cancer Res. *65*, 4020–4030.

Waters, C.A., Strande, N.T., Wyatt, D.W., Pryor, J.M., and Ramsden, D.A. (2014). Nonhomologous end joining: a good solution for bad ends. DNA Repair (Amst.) *17*, 39–51.

Woodbine, L., Gennery, A.R., and Jeggo, P.A. (2014). The clinical impact of deficiency in DNA non-homologous end-joining. DNA Repair (Amst.) *16*, 84–96.

Wu, P.-Y., Frit, P., Meesala, S., Dauvillier, S., Modesti, M., Andres, S.N., Huang, Y., Sekiguchi, J., Calsou, P., Salles, B., and Junop, M.S. (2009). Structural and functional interaction between the human DNA repair proteins DNA ligase IV and XRCC4. Mol. Cell. Biol. *29*, 3163–3172.

Xing, M., Yang, M., Huo, W., Feng, F., Wei, L., Jiang, W., Ning, S., Yan, Z., Li, W., Wang, Q., et al. (2015). Interactome analysis identifies a new paralogue of XRCC4 in non-homologous end joining DNA repair pathway. Nat. Commun. *6*, 6233.

Yoo, S., and Dynan, W.S. (1999). Geometry of a complex formed by double strand break repair proteins at a single DNA end: recruitment of DNA-PKcs induces inward translocation of Ku protein. Nucleic Acids Res. *27*, 4679–4686.

Yoo, S., Kimzey, A., and Dynan, W.S. (1999). Photocross-linking of an oriented DNA repair complex. Ku bound at a single DNA end. J. Biol. Chem. *274*, 20034–20039.

Zha, S., Guo, C., Boboila, C., Oksenych, V., Cheng, H.-L., Zhang, Y., Wesemann, D.R., Yuen, G., Patel, H., Goff, P.H., et al. (2011). ATM damage response and XLF repair factor are functionally redundant in joining DNA breaks. Nature *469*, 250–254.